Electronic Supplementary Information for the paper:

# Multivariate analysis coupled to infrared spectroscopy unravel the diversity of adsorption sites and strengths of a zeolite surface

Reda Aboulayt [a] Eleonora Vottero [a] Alexandre Vimont [a] Philippe Bazin [a] Emily Bloch [b] Sandrine Bourrelly,[b] Sylvie Maury [c] Céline Chizallet [c] and Arnaud Travert [*a]

[a] *Université de Caen Normandie, ENSICAEN, CNRS, LCS, 14000 Caen, France. E-mail: arnaud.travert@unicaen.fr*

[b] *UMR 7246: Laboratoire MADIREL, CNRS/Université Aix-Marseille, 52 avenue Escadrille Normandie – Niemen, 13013 Marseille, France. E-mail: sandrine.bourrelly@univ-amu.fr*

[c] *IFP Energies nouvelles, Rond-point de l'échangeur de Solaize, BP3, 69360, France. E-mail: celine.chizallet@ifpen.fr*

TABLE S1. Physicochemical properties of the MFI studied

| Zeolite | $S_{BET}$ ($m^2/g$) | $S_{EXT}$ ($m^2/g$) | $V_P$ ($cm^3/g$) | $V_\mu$ ($cm^3/g$) |
|---|---|---|---|---|
| MFI | 400 | 44 | 0.288 | 0.157 |

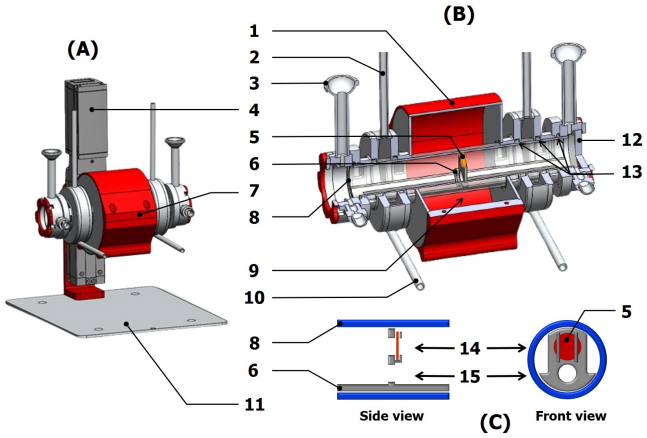


FIG. S1. General (A) and detailed (B) views of the "Jumpipe" IR cell. (C) Schematic drawing of the sample holder in quartz. 1 - External shell, 2 - Air cooling inlet, 3 - Connection for the vacuum apparatus, 4 - Motorized translation unit, 5 - Sample (wafer with a diameter of 13 mm), 6 - 2-positions sample holder, 7 - Removable IR cell, 8 - Quartz pipe, 9 - Oven location, 10 - Air cooling outlet, 11 - Spectrometer base-plate, 12 - KBr window for the IR beam, 13 - Kalrez O-rings, 14 - IR beam position for sample spectrum, 15 - IR beam position for gas phase spectrum (or background).

## SI. DETERMINATION OF ADSORPTION ISOTHERMS BY THE INTEGRATION METHOD

Spectroscopic isotherms were obtained by plotting the area of selected absorption bands vs iBuOH equilibrium pressure at different temperatures.

Difference spectra depicted in Figure S2 were used to highlight the changes occurring upon adsorption: negative bands correspond to the consumption of zeolitic OH groups ($\nu$(OH), 3800–3500 cm$^{-1}$) (Fig. S2-a) and positive bands to the characteristic vibrations of adsorbed iBuOH, in particular the $\delta(CH_2)$ region (Fig. S2-b). The integration windows targeted the silanols and bridging OH bands in the $\nu$(OH) region, as well as the $\delta(CH_2)$ band at 1470 cm$^{-1}$. The integration ranges were selected based on the characteristic spectral regions of the relevant vibrations (bridging OH, silanols and $\delta$(CH2) bands of adsorbed isobutanol), while avoiding overlapping regions whenever possible. A local baseline was defined on both sides of each band prior to integration, and the same integration limits were applied to the whole dataset to ensure consistent comparison of band areas across the spectra.

The EFAL–OH region ($\approx$ 3660 cm$^{-1}$) was not considered due to significant overlap with neighbouring bands.

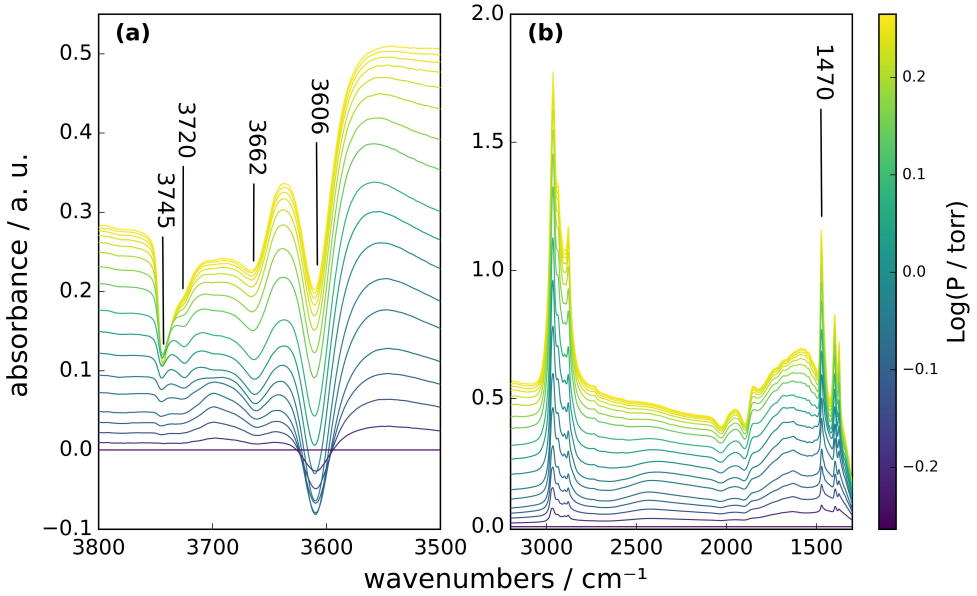


FIG. S2. Difference spectra of iBuOH/H-ZSM-5 in the $\nu$(OH) (a) and $\nu$(CH)-$\delta(CH_2)$ (b)

The integrated areas $A_i$ were plotted as a function of iBuOH partial pressure to obtain optical isotherms as shown in Figure S3. They were then fitted with four adsorption models.(Table S2)

Selection of the best models was made by considering the coefficient of determination $R^2$ (values between 0 and 1), which measures the adequacy between the fitted model and the experimental data (optical isotherms). However, the more adjustable parameters a model includes, the higher the $R^2$ coefficient. To overcome this bias, the adjusted coefficient of determination $R^2_{adjusted}$ were considered as they take into account the degree of freedom $n-p-1$ of the regression, where $n$ is the number of observations (experimental points) and $p$ the number of variable parameters of the model:

$$R^2_{adjusted} = 1 - \frac{n-1}{(n-p-1)}(1-R^2) \tag{S1}$$

The determination of $K_i$ at various adsorption temperatures allowed the determination of adsorption enthalpies and entropies using the van't Hoff equation:[S1]

$$\ln K = -\frac{\Delta_{ads}H^o}{RT} + \frac{\Delta_{ads}S^o}{R} \tag{S2}$$

The quality of fit was assessed by the $R^2_{adjusted}$ values summarized in Table S3. The corresponding adsorption parameters at 350 K are reported in Table S4, and the representative fitted curves are shown in Figure S4. Overall,

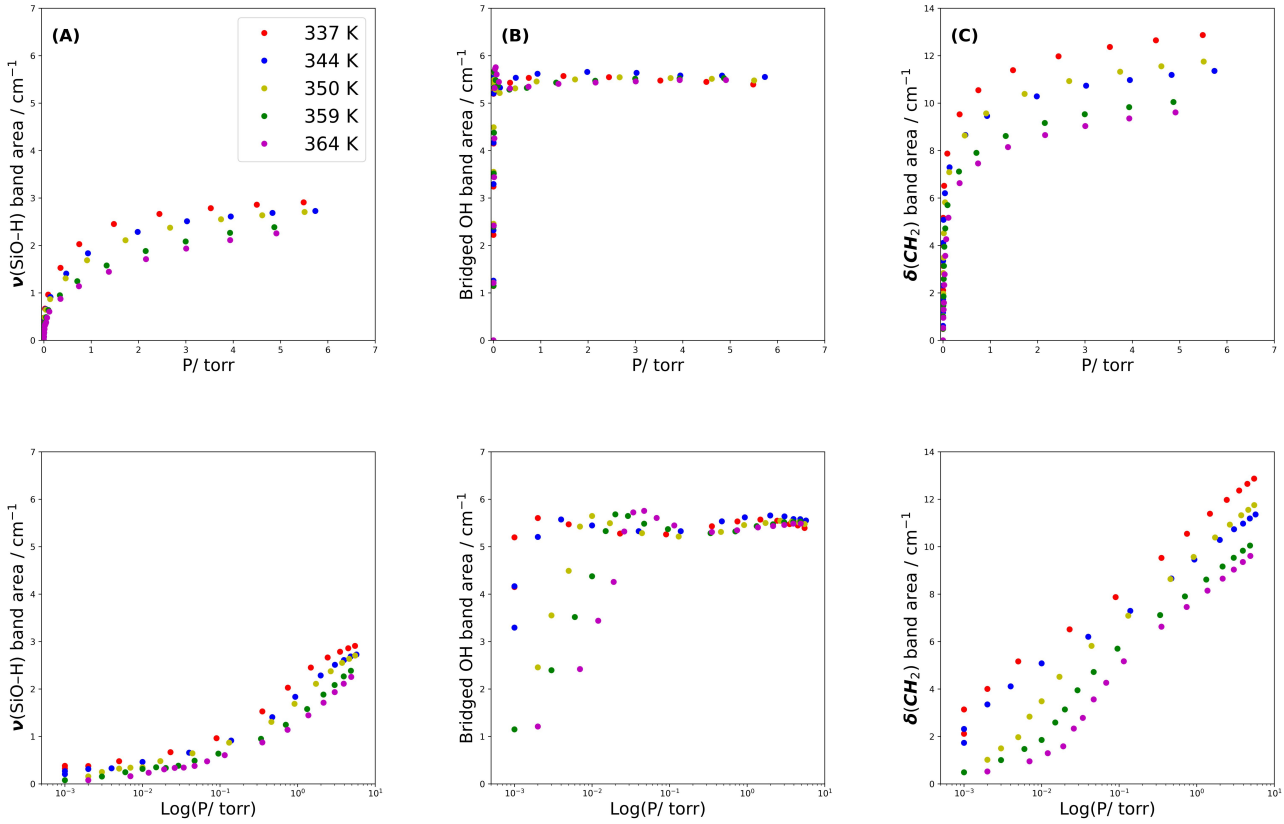


FIG. S3. Spectroscopic isotherms for iBuOH adsorption on H-ZSM-5 in (A) Silanols, (B) bridging OH and (C) $\delta(CH_2)$.Band areas obtained by integration for 10 mg of sample. Top: normal scale, bottom: Log scale.

TABLE S2. Adsorption isotherm models used in the study.

| Langmuir [S7] | Toth [S8] | Bi-Langmuir [S9] | Sips [S10] |
|---|---|---|---|
| $\theta_i = \dfrac{\mathbf{K}_i P}{1+\mathbf{K}_i P}$ | $\theta_i = \dfrac{\mathbf{K}_i P}{[1+(\mathbf{K}_i P)^t]^{1/t}}$ | $\theta_i = f\dfrac{\mathbf{K}_{1i} P}{1+\mathbf{K}_{1i} P} + (1-f)\dfrac{\mathbf{K}_{2i} P}{1+\mathbf{K}_{2i} P}$ | $\theta_i = \dfrac{\mathbf{K}_i (P)^{1/n}}{1+\mathbf{K}_i (P)^{1/n}}$ |

the fitted parameters fall within the ranges expected for alcohol adsorption on zeolitic hydroxyl sites, in agreement with literature values (Gómez-Álvarez et al.[S2],C.-C. Lee[S3],Nguyen et al[S4, S5],Thamm et al [S6])).

However, the methodology has limitations: the extra-framework aluminium region could not be studied, the $\delta(CH_2)$ spectra give relatively limited information and the integration can differ from a user to another which can lead to more errors (over/underestimation of the region to integrate). Further interpretation of site heterogeneity and enthalpy trends is discussed in the main text.

TABLE S3. $\mathbf{R}^2_{adjusted}$ from the integration method – Langmuir, Toth, Sips and Bi-Langmuir models reported at 350 K.

| | Silanols | bridging OH | iBuOH $\delta(CH_2)$ |
|---|---|---|---|
| Langmuir | 0.977 | 0.961 | 0.976 |
| Toth | 0.961 | 0.927 | 0.987 |
| Sips | 0.971 | 0.955 | 0.988 |
| Bi Langmuir | 0.983 \| 0.966 | N.A | 0.990 \| 0.986 |

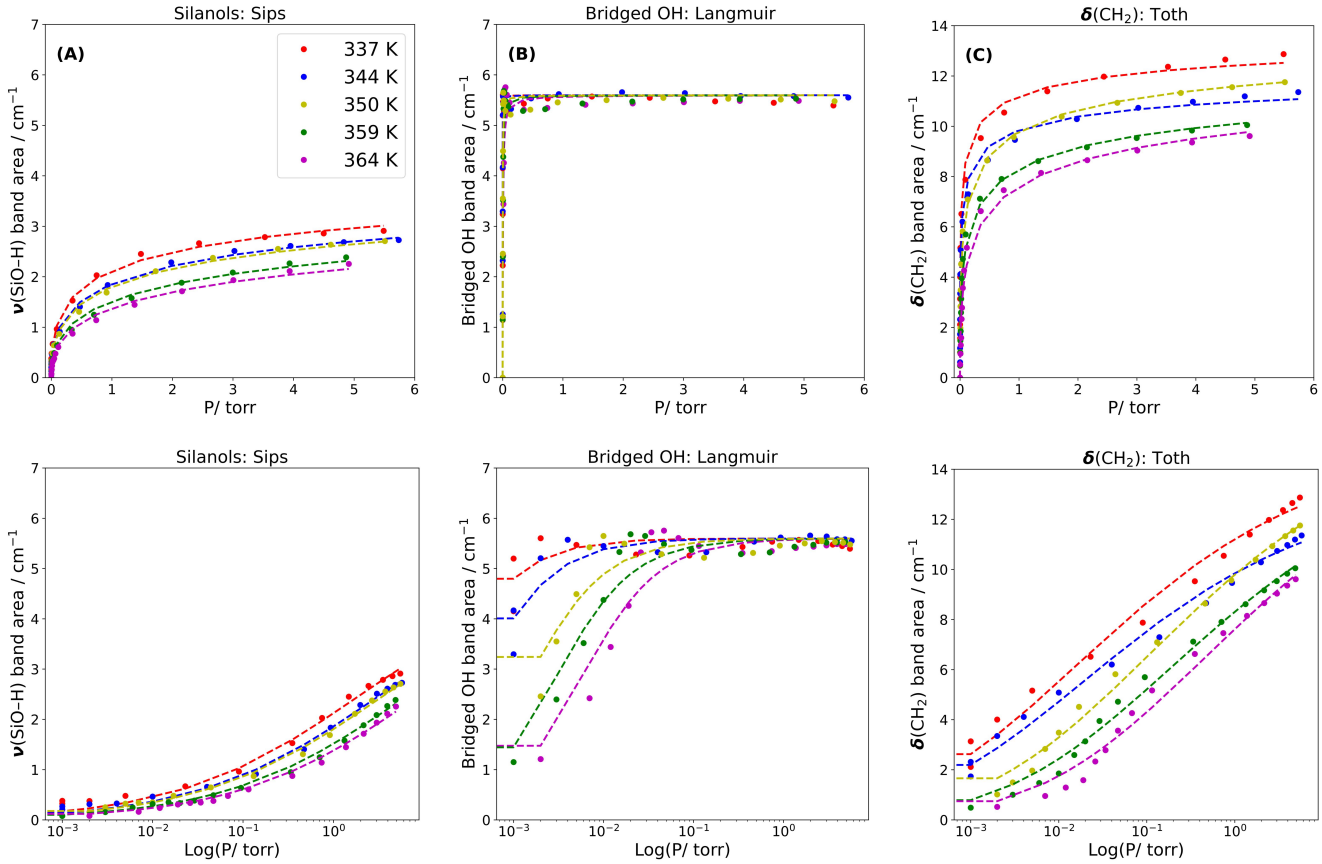


FIG. S4. Best spectroscopic isotherms adjustments for iBuOH adsorption on H-ZSM-5 in (A) Silanols, (B) bridging OH and (C) $\delta(CH_2)$ Band areas obtained by integration for 10 mg of sample. Top: normal scale, bottom: Log scale.

TABLE S4. Adsorption enthalpy values ($\Delta_{ads}H°$ / kJ/mol) at 351 K from the integration method for the iBuOH/H-ZSM-5 system fit with Langmuir, Bi-Langmuir, Sips and Toth models.

| $\Delta_{ads}H°$ kJ/mol | Silanols | bridging OH | Isobutanol uptake $\delta(CH_2)$ |
|---|---|---|---|
| Langmuir | -63 ± 4 | -136 ± 11 | -113 ± 7 |
| Toth | -52 ± 4 (t=0.19) | -121 ± 10 (t=1.3) | -111 ± 5 (t=0.33) |
| Sips | -57 ± 4 (1/n=0.42) | -129 ± 11 (1/n=1.24) | -110 ± 6 (1/n=0.44) |
| Bi-Langmuir | -125 ± 5 (18%)\|-56 ± 4 (82%) | N.A | -130 ± 10 (55%)\|-72 ± 2 (45%) |

## SII. MCR-ALS ANALYSIS

The Multivariate Curve Resolution by Alternating Least Squares (MCR-ALS) algorithm [S11] was used to extract detailed information about adsorbed species present both on the external surface and within the bulk of zeolite crystals. MCR-ALS constructs a bilinear model representing the experimental spectral matrix $\mathbf{D}$ as the product of concentration and spectral profiles. The corresponding matrices, $\mathbf{C}$ (concentration profiles) and $\mathbf{S}^T$ (spectral profiles) are iteratively optimised from an initial guess ($\mathbf{C}_0$ or $\mathbf{S}_0^T$) using an alternating least squares method to solve the matrix equation:

$$\mathbf{D} = \mathbf{C}\mathbf{S}^T + \mathbf{E} \tag{S3}$$

where $\mathbf{E}$ stands for the matrix of residuals (absorbance units) to minimise. The validity of the models was tested by comparing the original spectral matrix $\mathbf{D}$ with the reconstructed dataset $\hat{\mathbf{D}} = \mathbf{C}\mathbf{S}^T$.

In each iterative cycle of the optimization process, the concentration profiles were subjected to soft or hard-soft constraints. In the soft MCR-ALS approach, non-negativity and monotonicity with respect to pressure were enforced on the concentration profiles. Following this soft-constrained MCR-ALS optimisation, adsorption parameters were determined by fitting local isotherms to the final concentration profiles obtained, as described in the literature[S12, S13].

Alternatively, the hard-soft MCR-ALS strategy[S14] integrated isotherm fitting directly within the ALS optimisation loop. In this framework, local adsorption isotherms were iteratively adjusted on the least-square estimation of the concentration profiles, thereby decreasing the rotational ambiguity of MCR ALS.

The equations used for the local isotherms $\hat{\theta}_i\,(P, K_i, \ldots)$ covered Langmuir, Toth and Bi-Langmuir isotherms (Table S2) to optimize the adsorption parameters and were fitted to the surface concentration profiles $C_i\,(P)$:

$$(K_i, C_i^{\infty}, \ldots) = \underset{K_i, C_i^{\infty}, \ldots}{\arg\min} \sum_j \left[ \frac{C_i(P_j)}{C_i^{\infty}} - \hat{\theta}_i(P_j, K_i, \ldots) \right]^2 \tag{S4}$$

where $C_i^{\infty}$ is the estimate of the corresponding concentration at saturation, the experimental fractional coverage being given by :

$$\theta_i = \frac{C_i(P)}{C_i^{\infty}} \tag{S5}$$

All chemometric analyses were performed using the SpectroChemPy package.[S15].

Table S5 summarizes the equilibrium constants K obtained from soft and hard-soft MCR-ALS analyses, with the corresponding quality-of-fit indicators ($R^2$ and $R^2_{\text{adjusted}}$) reported at 350 K.

TABLE S5. $K$ ($\text{torr}^{-1}$) values for iBuOH adsorption on H-ZSM-5 from soft MCR-ALS for Langmuir and Toth models - Hard/Soft MCR-ALS for the Toth model. $R^2$ and $R^2_{\text{adjusted}}$ are reported at 350 K.

| Species | Model | 337 K | 344 K | 350 K | 359 K | 364 K | $R^2$ | $R^2_{\text{adjusted}}$ |
|---|---|---|---|---|---|---|---|---|
| Silanols | Langmuir | 3.973 | 2.761 | 1.585 | 0.919 | 0.955 | 0.989 | 0.975 |
| | Toth | 12.21 | 7.193 | 4.244 | 1.395 | 1.400 | 0.997 | 0.992 |
| | Hard/Soft Toth | 9.217 | 5.751 | 5.333 | 3.234 | 2.003 | N/A[(a)] | N/A[(a)] |
| EFAL OH | Langmuir | 385.8 | 117.4 | 68.77 | 34.89 | 16.51 | 0.979 | 0.949 |
| | Toth | 433.7 | 249.1 | 62.25 | 21.40 | 11.01 | 0.982 | 0.950 |
| | Hard/Soft Toth | 486.4 | 263.5 | 81.34 | 26.17 | 16.04 | N/A[(a)] | N/A[(a)] |
| Bridging OH | Langmuir | 4237 | 4336 | 1084 | 521.6 | 235.3 | 0.917 | 0.800 |
| | Toth | 3848 | 4312 | 1046 | 520.4 | 235.2 | 0.956 | 0.887 |
| | Hard/Soft Toth | 3100 | 2999 | 824.8 | 429.1 | 148.2 | N/A[(a)] | N/A[(a)] |

(a) Not Applicable for Hard/Soft MCR-ALS fits

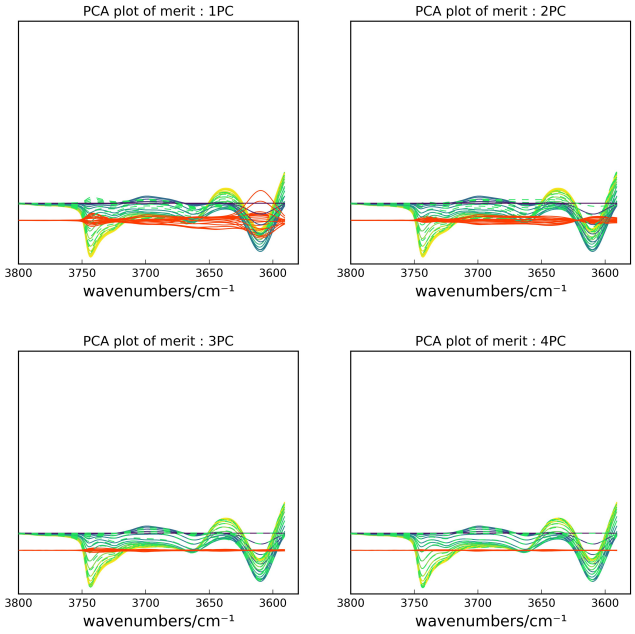


FIG. S5. PCA plot of merit for $n$ = 1,2,3 and 4 principal components (PC) for iBuOH/H-ZSM-5 at 350 K. It superimposes the reconstructed spectra $\hat{\mathbf{D}}_n$ with $n$ components (dashed line) to the experimental spectra $\mathbf{D}$ (full lines), along with the residuals $\mathbf{E}_n = \mathbf{D} - \hat{\mathbf{D}}_n$ (red lines).

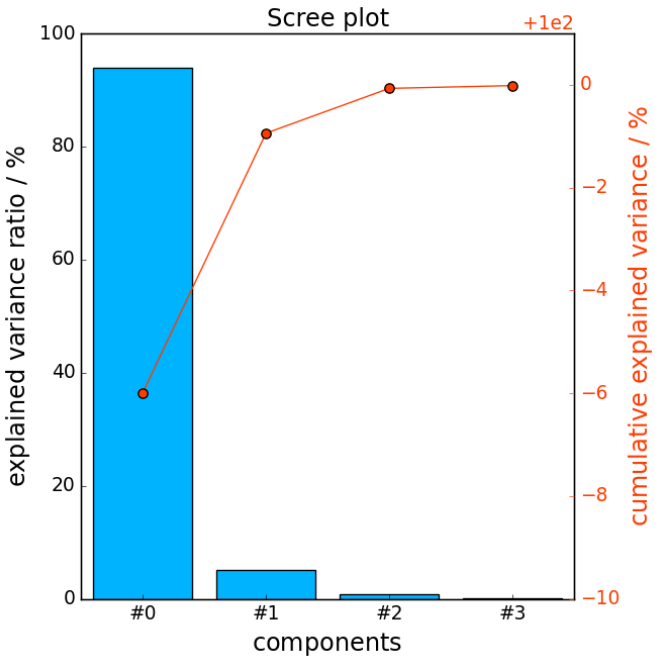


FIG. S6. PCA scree plot for 4 species- iBuOH adsorption on H-ZSM-5 at 350 K.

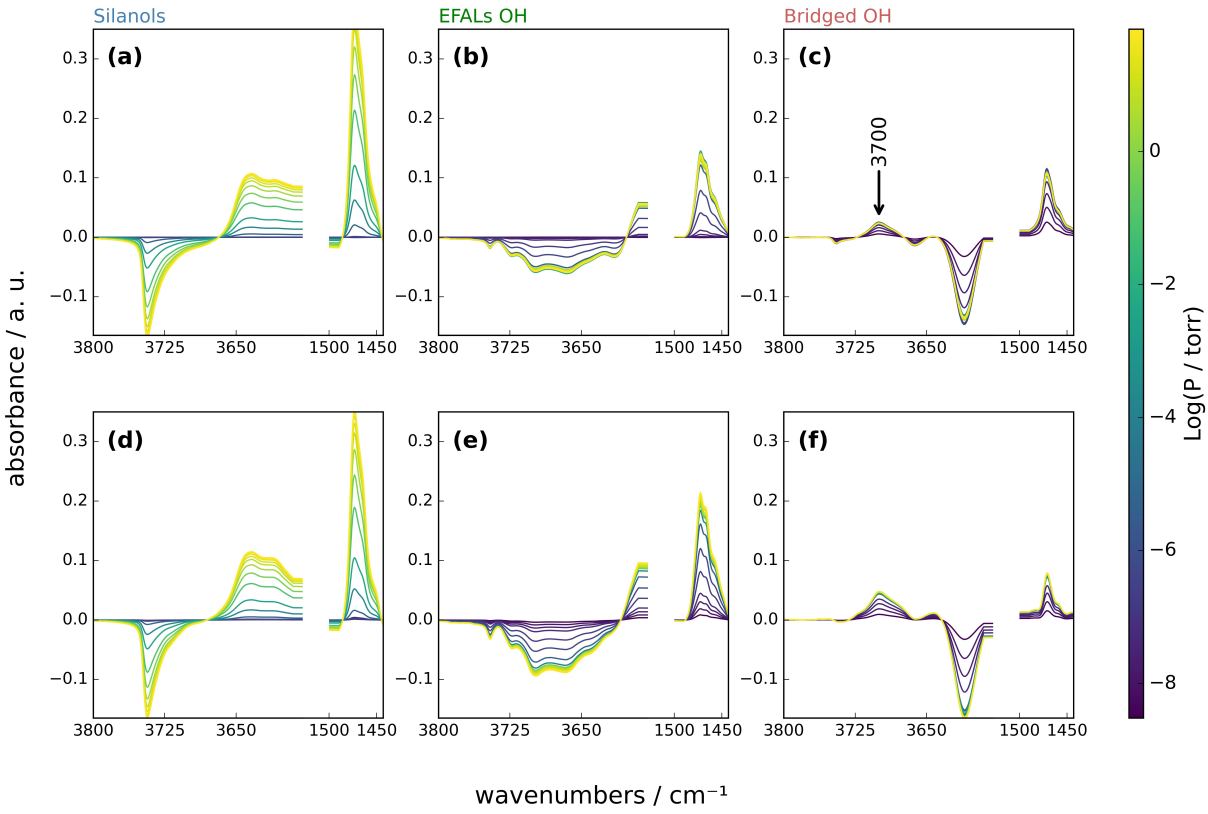


FIG. S7. Contribution of each species from MCR-ALS for iBuOH adsorption on H-ZSM-5 at 350 K. Soft constraints: Silanols (a), EFAL OH (b) and bridging OH groups (c) - hard/soft constraints: Silanols (d), EFAL OH (e) and bridging OH groups (f).

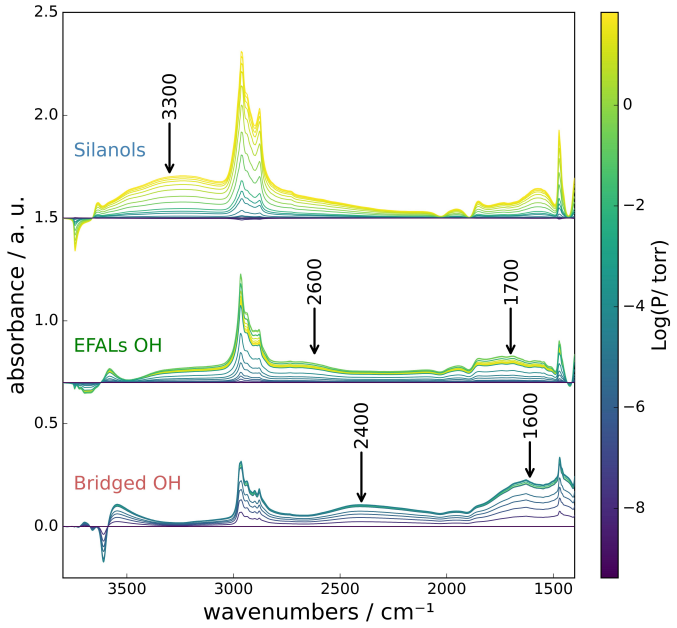


FIG. S8. Extended contribution of each species from soft MCR-ALS (iBuOH adsorption on H-ZSM-5 at 350 K).

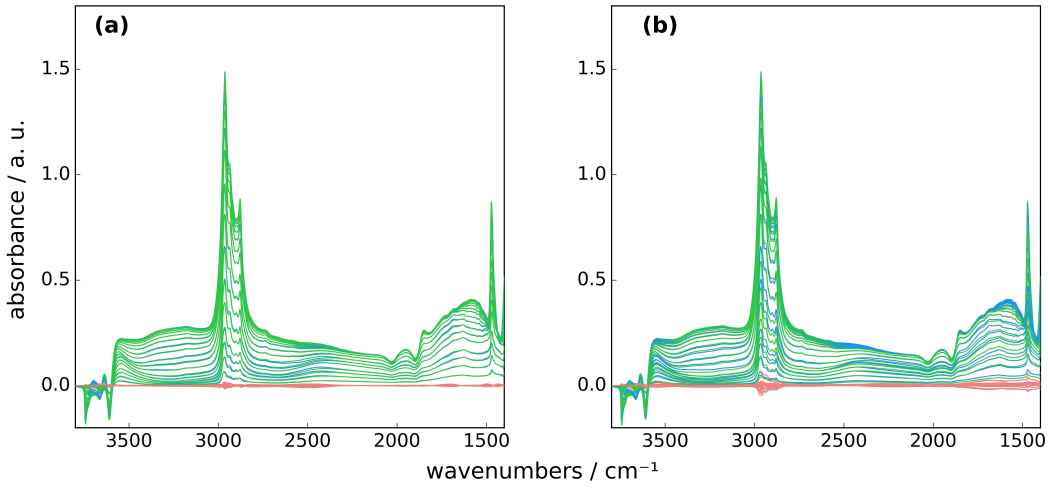


FIG. S9. Error in spectrum reconstruction over the entire pressure range for soft MCR-ALS (a) vs hard-soft (b) (iBuOH adsorption on H-ZSM-5 at 350 K).

## SIII. COMPLEMENTARY STRUCTURES CALCULATED BY DFT

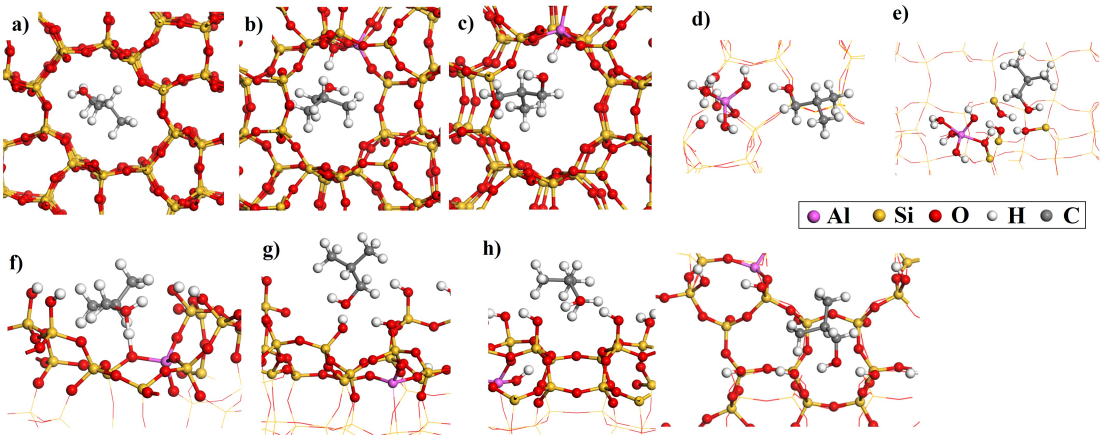


FIG. S10. Optimized structures by DFT calculations of some of the systems considered in the present work, isobutanol adsorption a) at the straight channel of bulk silicalite-1, b) at the sinusoidal channel of bulk ZSM-5, c) at the intersection of channels in bulk ZSM-5, d) at the Al-OH site of the EFAl, e) at the silanol nest close to the EFAl, f) at a surface bridging OH group, with an adsorption mode co-involving a silanol group, g) at a surface silanol group, h) between two surface silanol groups, left: side view, right: top view.

[S1] S. A. Kantonen, N. M. Henriksen and M. K. Gilson, Biochim. Biophys. Acta - Gen. Subj., 2018, **1862**, 692–704.
[S2] P. Gomez-Alvarez, E. G. Noya, E. Lomba, S. Valencia and J. Pires, Langmuir, 2018, **34**, 12739–12750.
[S3] C.-C. Lee, R. Gorte and W. Farneth, J. Phys. Chem. B, 1997, **101**, 3811–3817.
[S4] C. M. Nguyen, M.-F. Reyniers and G. B. Marin, J. Phys. Chem. C, 2011, **115**, 8658–8669.
[S5] C. M. Nguyen, M.-F. Reyniers and G. B. Marin, J. Catal., 2015, **322**, 91–103.
[S6] H. Thamm, J. Chem. Soc., Faraday Trans. 1, **85**, 1–9.
[S7] I. Langmuir, J. Am. Chem. Soc., 1915, **37**, 1139–1167.
[S8] J. Tóth, Acta Chim. Hung., 1971, **69**, 311–328.
[S9] R. T. Yang, Gas separation by adsorption processes, World Scientific, 1997, vol. 1.
[S10] R. Sips, J. Chem. Phys., 1948, **16**, 490–495.
[S11] A. de Juan, J. Jaumot and R. Tauler, Anal. Methods, 2014, **6**, 4964–4976.
[S12] J. Serafin and B. Dziejarski, Micropor. Mesopor. Mat., 2023, **354**, 112513.
[S13] H. Swenson and N. P. Stadie, Langmuir, 2019, **35**, 5409–5426.
[S14] A. de Juan, M. Maeder, M. Martinez and R. Tauler, Chemom. Intell. Lab. Syst., 2000, **54**, 123–141.
[S15] A. Travert and C. Fernandez, SpectroChemPy, 2025, `https://zenodo.org/doi/10.5281/zenodo.3823841`, (accessed: February 10, 2025).